Influence of surface roughness on secondary electron emission from graphite

Thomas S. BurtonTyson C. BackSteven B. FairchildGregory B. Thompson

Citation: Journal of Vacuum Science & Technology A: Vacuum, Surfaces, and Films **35**, 041404 (2017); doi: 10.1116/1.4986629

View online: http://dx.doi.org/10.1116/1.4986629

View Table of Contents: http://avs.scitation.org/toc/jva/35/4

Published by the American Vacuum Society

Influence of surface roughness on secondary electron emission from graphite

Thomas S. Burton
Department of Metallurgical and Materials Engineering, University of Alabama, Tuscaloosa, Alabama 35487

Tyson C. Back
Materials and Manufacturing Directorate, Air Force Research Laboratory, Dayton, Ohio 45433
and University of Dayton Research Institute, University of Dayton, Dayton, Ohio 45469

Steven B. Fairchild
Materials and Manufacturing Directorate, Air Force Research Laboratory, Dayton, Ohio 45433

Gregory B. Thompson[a)]
Department of Metallurgical and Materials Engineering, University of Alabama, Tuscaloosa, Alabama 35487

(Received 7 April 2017; accepted 5 June 2017; published 15 June 2017)

In this study, the authors address how surface roughness alters secondary electron emission. By using specific grades of metallographic polishing pads, controlled levels of roughness and surface features were imparted. As expected, the smoothest surface (root mean square roughness $0.110 \pm 0.022\,\mu$m) produced the highest secondary electron yield; however, a moderate rough surface ($0.990 \pm 0.019\,\mu$m) produced a slightly lower yield as compared to a rougher surface ($7.10 \pm 1.23\,\mu$m) at lower primary electron energies. This inversion, that a macroscopic rougher surface yields a higher emission, has been explained by differences between large and small scale variations in the surface roughness and the frequency that these features appeared on the surface. The surface roughness was quantified using optical profilometry and a fast Fourier transform of the surface topology. © *2017 American Vacuum Society*. [http://dx.doi.org/10.1116/1.4986629]

I. INTRODUCTION

Graphite has been used in a variety of low and high plasma density field studies[1,2] in applications such as traveling wave tubes[3–5] and chamber walls for fusion reaction plasmas.[6–8] Graphite has also been considered for use as a containment system for plasmas in Hall effect thrusters.[9] In all cases, the secondary electron emission (SEE) from the graphite surface regulates the plasma sheath stability. The plasma sheath is the boundary layer between the charge neutral portion of a plasma and its charge transition that forms near the surface. As plasma particles bombard a surface, the surface erodes creating a variation in topologies, which will alter the surface emission characteristics which in turn influence the plasma sheath. Langendorf and Walker[10] have recently reported how the plasma sheath potential became altered between a "rough" and "smooth" hexagonal boron nitride (hBN) surface although the extent of the surface morphology change was not quantified. Although hBN has a higher value for general emission than graphite,[11,12] the influence of surface morphology on emission has been observed and should also exist for a graphite surface. This study aims at exploring this structure-property effect.

The variation of surface features should dramatically change the electron emission characteristics. This includes the re-emitted secondary electrons (SEs) and back scattered electrons from the surface that regulates the space-charge stability for a plasma sheath. If the surface electron emission changes, the plasma sheath will be altered, which in turn varies how the plasma interacts with the surface. Thus, understanding the ways in which surface topological variations modify these electron emission values would then allow for more comprehensive knowledge of how they might influence plasma sheath–surface interactions. Such information would, for example, be useful in identifying the extent of plasma-based erosion in materials as a function of evolving surface morphology.[1,2]

In a typical electron emission study, a primary electron beam is focused onto the surface whereupon the emitted surface electrons are captured.[13] If the sample is a dielectric, the surface will charge and repel the primary electron beam, and such measurements cannot be acquired. Means to overcome this experimental challenge have included pulsing the primary electron beam to allow the surface to dissipate the charge build up.[14] Depending on the experimental setup, this can be an arduous experiment to ensure that all the surface charge is dissipated prior to the next beam exposure. In contrast, a high electrical conductive sample does not suffer from these issues and can readily provide emission data in either a continuous or pulse beam condition. Consequently, one of the key advantages of using graphite for such surface morphology studies, as compared to other more insulating materials such as hBN, alumina, or silica, is its high electrical conductivity ($15.5\,\mu\Omega\,\mathrm{m}^{-1}$).[15]

Although several studies have been conducted on the measurement of SEE from various material types,[12,14] to date, there has been little work in quantifying how the surface morphology of such materials influences electron emission. In this paper, we have systematically roughened a graphite surface through various metallographic preparation steps. In this manner, the surface roughness was repeatable

[a)]Electronic mail: gthompson@eng.ua.edu

and uniform over the surface as well as having roughness values that could scale over multiple orders of magnitude. After which, the micro- and macrolength scale effects of the roughness on the emission behavior could be ascertained.

II. EXPERIMENT

A. Sample preparation

EC-17 grade, ultrafine grain electro discharge machining graphite was chosen as the case study material. This graphite was acquired from Tokai Carbon where it was isostatically pressed and sintered with a resulting average grain size of approximately 2 μm with a density of 99 $\pm$ 0.5%. Graphite was sectioned into approximately 1×1 cm squares with thicknesses of approximately 5 mm.

The samples were mounted into 3.175 cm cold mount pucks using a Buehler SamplKwik acrylic cold mounting system, which were then cut out of the mount postgrinding or polishing. For the samples denoted as polished, they were all prepared to a final polish using a 0.05 μm alumina-based aqueous solution. The two roughened graphite samples had their surfaces mechanically attrited with either a 120 grit ($\sim$125 μm particulate diameter) or 1200 grit ($\sim$15.3 μm particulate diameter) SiC metallographic grade paper. Postgrinding/polishing, all the samples were cleaned of any surface contaminates by ultrasonic vibration in acetone followed by rinsing with isopropanol and deionized water and finally dried under compressed air. X-ray photo-spectroscopy (XPS) performed in a Kratos Axis 165 XPS/Auger confirmed the removal of any polishing containments prior to secondary electron yield (SEY) measurements.

B. Sample roughness characterization

The sample surfaces were imaged by scanning electron microscopy (SEM) using a JEOL 7000 at 1000$\times$ magnification at a working distance of 10.0 mm and an acceleration voltage of 10 keV in the SE imaging mode. Optical profilometry, to quantify the roughness, was performed by Evan's Analytical Group using a Bruker Contour GT-X8 with a 50$\times$ optical lens. Three 1.3×0.95 mm areas were scanned from each sample where each scan had a vertical resolution of 6 nm and a lateral resolution of 6 μm. Roughness statistics were then collected across the entire scanned surfaces with root mean square (RMS) roughness (S_q), given below, as the primary statistic considered

$$S_q = \sqrt{\frac{\Sigma(z_i - z_{avg})^2}{N}}, \tag{1}$$

where Z_i is the height of the feature, Z_{avg} is the average Z value within the scanned image, and N is the number of points in the image. For comparison to other roughness analytical methods, the geometric mean or average surface roughness (S_a) has also been calculated and is given as

$$S_a = \frac{\Sigma z_i}{N}. \tag{2}$$

Discrete Fourier transforms were calculated from the optical profilometry height data using a MATLAB© code. This program calculated the discrete Fourier transform of a vector, treating the columns of the height map data matrix as the vectors. Each column was conditioned using two steps prior to running the transform. First, the dc offset was removed by subtracting the mean height of each column. Then, a Hanning window was applied to each set, correcting for discontinuities in the height signal. The height data matrix was transposed to form a matrix of dimensions 480×640, which produced 640 individual transforms which are then averaged together. This orientation was selected to provide additional blocks of data necessary for averaging the orientation of deformities quantified in the optical profilometry data. The frequency for each bin returned by the fast Fourier transform was found using the dimensions of the profilometry data. The dimensions were 0.95×1.3 mm, which yielded a sampling frequency of approximately 505 samples/mm. This in turn yielded a Nyquist frequency of 252.5 occurrences/mm and a bin size of approximately 1.03 occurrences/mm.

C. Sample emission measurements

The secondary electron emission coefficient was collected in a custom constructed stainless steel vacuum chamber at a base pressure of approximately 3×10^{-10} Torr pumped by mechanical and turbomolecular pumps, with the electron current being measured using a Keithley 6517A electrometer. A primary electron beam was rastered across each sample at normal incidence at accelerating voltages between 200 and 400 eV at 100 eV step sizes. The sample itself acted as the detector in this experimental setup. The electron current was first measured while the samples were under only primary electron beam irradiation (no bias), after which each measurement was repeated while the sample was charged to +100 V bias to recollect all the escaping secondary electrons that were emitted from the surface over a range of angles back into the sample. The net current of recollected electrons (i_n) and the current from the primary electron beam (i_p) are then used to calculate the SEY coefficient (δ) from

$$\delta = 1 - \left(\frac{i_p}{i_n}\right). \tag{3}$$

The value of (i_n), (i_p), and δ was collected once every 5 s for 600 s, and the value of δ, at an accelerating voltage, was the average of the last twenty values. The error for this energy level was also calculated from the same set of values.

III. RESULTS AND DISCUSSION

The SEM micrographs and optical profilometry height maps of the graphite samples can be seen in Fig. 1. From these images, one can easily discern the ever increasing level of surface roughness. At the largest roughness, the clear and coarse polishing lines are evident within the surface. At all levels of polishing, the graphite revealed jagged features which will be termed flaking in this paper. The

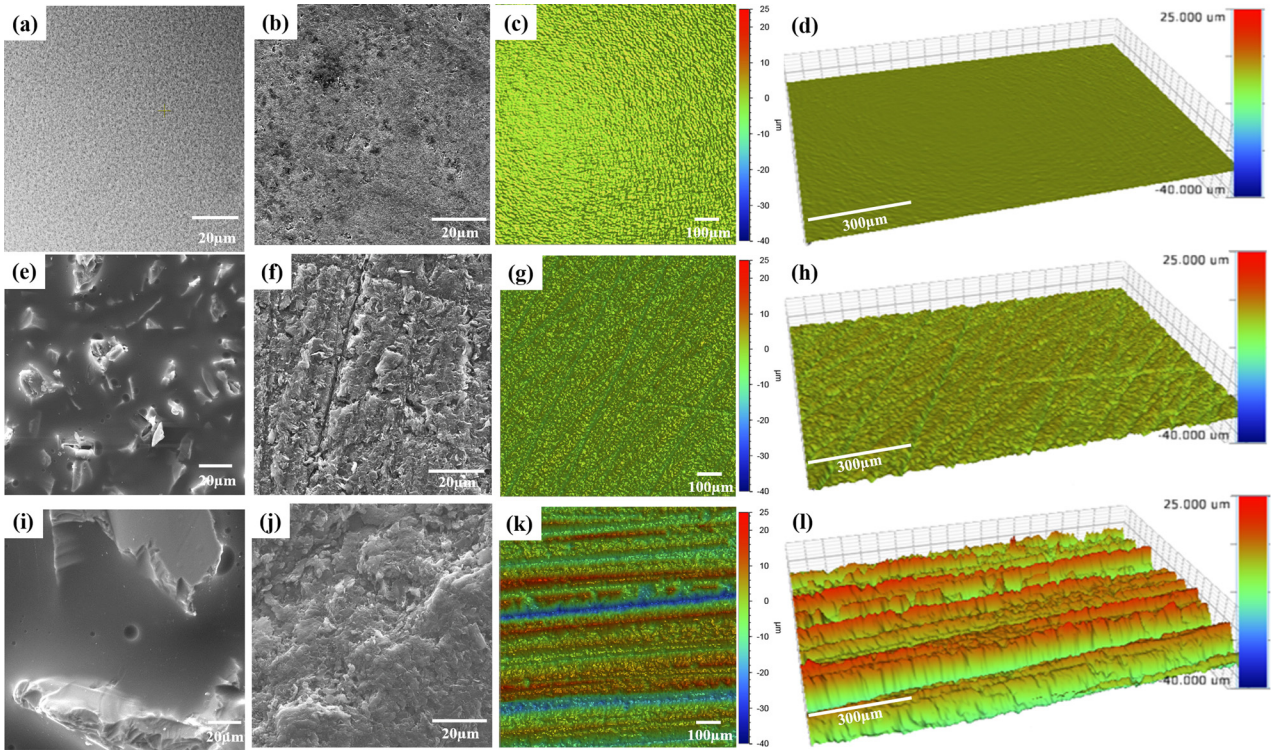

FIG. 1. (Color online) (a) JEOL 7000 secondary electron micrograph of the 0.050 μm silica spheres used to polish the smooth graphite surface, (b) secondary electron micrograph of the polished graphite surface, and (c) optical profilometry plan view and (d) 3D map of the polished graphite surface ($S_q = 0.110\,\mu$m). (e) Secondary electron micrograph of the 1200 grit SiC polishing pad, (f) micrograph of the 1200 grit graphite surface, and optical profilometry (g) plan view and (h) 3D map of the 1200 grit graphite surface ($S_q = 0.990\,\mu$m). (i) Secondary electron micrograph of the 120 grit SiC polishing pad and (j) micrograph of the 120 grit graphite surface; optical profilometry (k) plan view and (l) 3D Map of the 120 grit graphite surface ($S_q = 7.10\,\mu$m).

RMS roughness (S_q) and the average roughness (S_a) of the graphite surfaces are tabulated in Table I.

The SEY coefficient as a function of primary electron beam energy and surface roughness is plotted in Fig. 2. As to be expected, the polished (smoothest) graphite surface ($S_q = 0.110\,\mu$m) had the highest SEY coefficient, with a maximum value near 300 eV. The smooth, planar surface provided the conditions where the vast majority of electrons were able to emit unobstructed from the surface and contribute to the measurement. The two roughened surfaces exhibited a decrease in emission from the smooth surface with equivalent emission values at primary beam energies greater than ~350 eV. Although these surface roughness values are an order of magnitude different, at higher beam energies, the scale of the roughness does not seem to contribute to emission differences. However, upon decreasing the primary beam energy, a deviation in emission was found, with the roughest surface—graphite 120 grit ($S_q = 7.10\,\mu$m)—having a slightly higher emission than the graphite 1200 grit ($S_q = 0.990\,\mu$m). In the inset in Fig. 2, the standard deviation error at the 300 eV primary beam energy is shown, confirming that this difference is statistically significant. As all the graphite material used here was from the same source and tested in the same unit, with the only difference being the surface preparation, the variance in emission is likely linked to the character of the surface features themselves.

From these scans, it appears that a critical length scale influences the SEY coefficient when the primary beam energy is sufficiently low. One could assume that the rougher the

TABLE I. RMS roughness (S_q) and average roughness (S_a) of various graphite surfaces.

Graphite surface	RMS roughness [S_q] (μm)	Average roughness [S_a] (μm)
120 grit	7.10 ± 1.20	5.60 ± 0.842
1200 grit	0.990 ± 0.019	0.780 ± 0.022
Polished	0.110 ± 0.022	0.070 ± 0.004

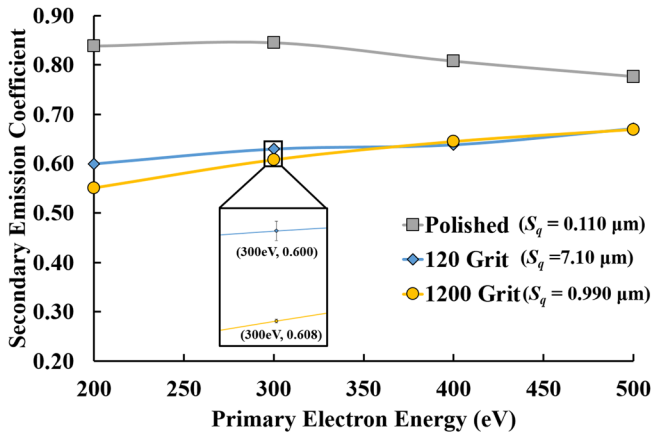

FIG. 2. (Color online) Plot of the measured secondary electron yield coefficient for the graphite samples at each energy level. Note that the roughest sample, 120 grit, does not correspond to the lowest emission response. The inset shows the low level of error found in the measurement technique.

surface, the lower the SEY would be as more of the surface variation could obstruct emission. Nonetheless, this is not the case. The roughest graphite 120 grit surface ($S_q = 7.10\,\mu$m) has a higher SEY coefficient value than the graphite 1200 grit surface ($S_q = 0.990\,\mu$m).

Langendorf[16] reported a ray trace model for electron trapping as a function of modulated topologies to investigate this type of behavior. In his model, as the depth of a groove increased, the probability of an emitted electron to escape the groove decreased because it had a greater opportunity to collide and be absorbed by the side walls within the groove. Similarly, if the spacing between grooves decreased, then the emission would decrease, for a fixed groove depth, because less surface area above the groove would be present to emit. This model is in agreement with experimental and modeling of silver and copper surfaces that were arranged as cylindrical wells in the study by Ye *et al.* In this study, a reduction of SEY occurred for an increasing aspect ratio of cylinder diameter to cylinder depth.[17]

To illustrate how these geometric surface effects relate to our roughened surfaces, we have plotted how the average roughness changed as a function of the analyzed partitioned area, Fig. 3, with the error being the standard deviation about the average roughness taken from each partitioned size. As the partitioned area decreased, which is equivalent to a reduced field of view with respect to the scale of roughness on the surface, the differences between the two roughest surfaces decreased. For the smoothest surface, as the sampling area or partition size decreased, very little change in roughness occurred meaning that at all length scales measured (small and larger fields of view), the surface is relatively uniform in its roughness. Returning to the rougher surfaces (120 and 1200 grit), their reduction in average roughness with the length scale infers that at finer feature sizes, the average surface roughness is less. However, the large error bars within each partition size does indicate dramatic variations from the sampled region to the next sampled region. By considering the average value for each partition size, the onset for this notable reduction in average roughness occurred at approximately 10^3 and $10^4\,\mu$m^2 for the 1200 and 120 grit conditions, respectively. At a partition size of $10^2\,\mu$m^2, the RMS roughness between the two surfaces is statistically equivalent (overlapping error bars) and may explain why, at higher primary beam energies, the two surfaces exhibit equivalent emission coefficients.

Returning to Langendorf's ray trace model mentioned previously, where the trapping of electrons is shown to be a function of groove depth and groove density, we can now understand why this rougher surface was able to emit more electrons at the lower primary energies. Since both surfaces, at the lowest partition size (field of view), exhibit similar RMS roughness values, Fig. 3, the difference in emission is likely attributed to the spacing of the grooves created by the polishing lines. Such an effect can be inferred from the optical profilometry scan of the 120 grit surface in Fig. 1(i). Large scale polish lines can be seen in this image. These features are formed from the larger particulates used in the 120 grit paper, shown in Fig. 1(g). Although these particulates are larger and yield a rougher surface with deeper polishing grooves, their size does leave a relatively smoother surface between the coarse polishing lines. This is manifested in the Fourier transform of its surface, Fig. 4, where at low frequencies (larger wavelengths), a higher number of peaks are observed.

Unlike the 120 grit polishing paper, the 1200 grit polishing paper, with its particulates shown in Fig. 1(d), was finer and created a closer spacing of polishing lines which translated to a higher density of grooves. This effect is also noted in the Fourier transform of Fig. 4 where the 1200 grit sample does not contain a significant distribution of pronounced peaks at the lower frequencies. Even though these 1200 grit grooves were not as deep (rough) as the 120 grit, they were sufficient to create surface modulations to trap electrons. Thus, by having a higher fraction of these grooves, it had a more pronounced effect on reducing the emission for the lower energy electrons. As the primary energy value increased, the electrons now had sufficient energy to overcome these surface obstructions and emit.

The reason for the significant differences between the polished graphite and the roughened graphite can also be

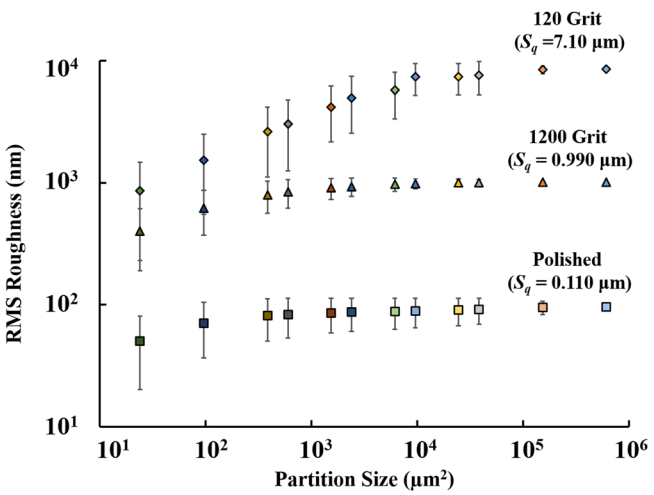

FIG. 3. (Color online) Roughness as a function of the reduced binned area for the analyzed graphite samples.

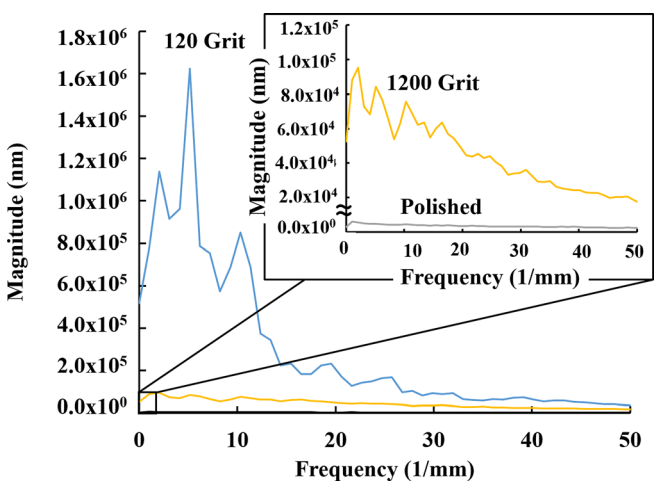

FIG. 4. (Color online) Fast Fourier transform of the optical profilometry height data to observe the regularity of surface features across its surface.

gleaned from Fig. 3. Even though the polished surface would have polishing lines or grooves, the depth and spacing of these features became less pronounced between these two geometric features. The roughness of this surface as well as the magnitude of Fourier transformed identified peaks (inset image in Fig. 4) was at least 1 order of magnitude lower than either rough surface. Even more notably, the surface roughness was constant over the reduce partition sizes in Fig. 3. Thus, this surface was much more smooth and able to emit electrons over all its area with little to no obstructions from the surface topology.

Comparing our results to a previous study,[11] our SEY values were found to be lower. Unfortunately, in the study by Balcon *et al.*, the grade and roughness of the graphite were not provided and may explain the discrepancy between our findings and their findings. Thus, reporting surface roughness as part of SEY studies, particularly at lower energies, may be useful for the community in the need to carefully quantify the surface morphology effects on measured emissions.

Finally, we note the convergence trend of the measured SEE coefficients with increasing primary electron energy. As the primary electron beam energy increased, the samples were able to emit electrons that originate deeper within the samples' themselves. Moreover, these emitted electrons will have higher energies because they are able to escape from the sample even though they originated further beneath the surface. Since the sample was single phase graphite, differences in this emission because of composition are not present. However, with ever increasing primary electron beam energy, the emission of these electrons increases whereupon they can dominate the signal from the electrons that are only emitted from the surface or very near surface interactions. The convergence of the SEE coefficients for the two roughest surfaces at energies greater than $\approx$350 eV demonstrates that such variations in roughness are no longer dominate as compared to the electrons that are emitted under the surface. Interestingly, the smoothest sample still maintains a higher SEE coefficient than the other two samples even up to the measured 500 eV primary electron beam energy. This does suggest that surface roughness can still have an impact on this coefficient at higher beam energies.

IV. SUMMARY AND CONCLUSIONS

This study investigated how surface roughness influenced the SEE behavior in graphite. It was found that the smoothest surface yielded the highest SEY. This was expected because such a surface would have very limited obstructions for electron emission. However, the roughest surface did not have the lowest SEY for the lowest electron energies; rather, a surface with moderate roughness yielded a lower emission. At sufficiently high electron beam energies ($\gtrsim$350 eV), the emission between these two roughened graphite surfaces became equivalent.

This emission difference for lower energies between the two roughened surfaces was understood in terms of a reduction in the macroscopic roughness values as a function of a finer field of view as well as the spacing of the grooves that created the roughness. Specific to this work, the roughest 120 grit graphite surface had a noticeable change in the mean roughness value when the partition size was $<10^4\ \mu m^2$ as compared to $<10^3\ \mu m^2$ for the 1200 grit surface. At a partition size of $10^2\ \mu m^2$, the roughness between the two surfaces was statistically equivalent. The Fourier transform of these roughened and polished surfaces revealed the notable presence of peaks at lower frequencies for the 120 grit surface, whereas a more uniform distribution of peak heights was quantified in the 1200 grit and polished surfaces.

Collectively, these geometric considerations suggested that a critical length scale in terms of roughness existed for the SEY for lower energy emitted electrons. Once these variations were minimized, as in the case of the polished surface, the emission became more uniform across the surface and exhibited a higher SEY. Quantifying surface roughness may also explain differences in SEY from equivalent materials reported by different groups.

ACKNOWLEDGMENTS

The authors would like to gratefully acknowledge the support of Grant No. AFOSR-FA9550-11-1-0160 and Abhishek Kumar and Tyler Brooker for their technical assistance.

[1]N. Gascon, M. Dudeck, and S. Barral, Phys. Plasmas **10**, 4123 (2003).
[2]S. Barral, K. Makowski, Z. Peradzyński, N. Gascon, and M. Dudeck, Phys. Plasmas **10**, 4137 (2003).
[3]D. Shiffler, J. Nation, L. Schachter, J. Ivers, and G. Kerslick, J. Appl. Phys. **70**, 106 (1991).
[4]A. Curren and T. Fox, IEEE Electron Device Lett. **2**, 252 (1981).
[5]R. Kompfner, Rep. Prog. Phys. **15**, 275 (1952).
[6]G. Federici *et al.*, Nucl. Fusion **41**, 1967 (2001).
[7]T. Yamashina and T. Hino, Appl. Surf. Sci. **48**, 483 (1991).
[8]R. Hawryluk *et al.*, Phys. Plasmas **5**, 1577 (1998).
[9]D. M. Goebel, R. R. Hofer, I. G. Mikellides, I. Katz, J. E. Polk, and B. N. Dotson, IEEE Trans. Plasma Sci. **43**, 118 (2015).
[10]S. Langendorf and M. Walker, Phys. Plasmas **22**, 033515 (2015).
[11]N. Balcon, D. Payan, M. Belhaj, T. Tondu, and V. Inguimbert, IEEE Trans. Plasma Sci. **40**, 282 (2012).
[12]P. Dawson, J. Appl. Phys. **37**, 3644 (1966).
[13]A. Shih, J. Yater, C. Hor, and R. Abrams, Appl. Surf. Sci. **111**, 251 (1997).
[14]V. Viel-Inguimbert, "Secondary electron emission of ceramics used in the channel of SPT," in *28th International Electric Propulsion Conference*, Toulouse, France (2003).
[15]Tokai Carbon Co., Ltd., "Isotropic graphite—Fine carbon," retrieved 24 October 2016, http://www.tokaicarbon.co.jp/en/products/fine_carbon/isotropic.html.
[16]S. J. Langendorf, *Effects of Electron Emission on Plasma Sheaths* (Daniel Guggenheim School of Aerospace Engineering, Georgia Institute of Technology, 2015).
[17]M. Ye, Y. N. He, S. G. Hu, R. Wang, T. C. Hu, J. Yang, and W. Z. Cui, J. Appl. Phys. **113**, 074904 (2013).